Analytical Biochemistry 507 (2016) 58–65

Contents lists available at ScienceDirect

Analytical Biochemistry

journal homepage: www.elsevier.com/locate/yabio

Sirtuin 1 evaluation with a novel immunoassay approach based on TiO_2–Au label and hyperbranched polymer hybrid

Yarui An

College of Science, University of Shanghai for Science and Technology, Shanghai 200093, People's Republic of China

ARTICLE INFO

Article history:
Received 3 March 2016
Received in revised form
10 May 2016
Accepted 21 May 2016
Available online 2 June 2016

Keywords:
SirT1
TiO_2–Au nanocomposite
Hyperbranched polymer
Electrochemical
Immunoassay

ABSTRACT

Accurate and highly sensitive evaluation of the sirtuin 1 (SirT1) level is becoming increasingly important for understanding the contribution of SirT1 in metabolism pathways. Here, a novel electrochemical immunoassay of SirT1 based on crosslinked hyperbranched azo-polymer decorated with gold colloids (Au–HAP) as sensing platform and titanium dioxide (TiO_2)–Au nanocomposites to immobilize secondary antibody–horseradish peroxidase (Ab_2–HRP) as electrochemical labels has been designed. Greatly enhanced sensitivity was achieved by exploiting the excellent conductivity of Au nanoparticle, the amplification effect of Au–HAP and TiO_2–Au, and the favorable catalytic ability of HRP. The nanocomposites of Au–HAP and TiO_2–Au could attach numerous capture antibodies on the surface for significant immune recognition efficiency. Meanwhile, the TiO_2–Au-labeled Ab_2–HRP using an HRP–thionine–H_2O_2 (hydrogen peroxide) detection system could further induce signal readout. Under optimal conditions, the signal intensity was linearly related to the concentration of SirT1 in the range of 1–500 ng ml^{-1}, and the limit of detection was 0.28 ng ml^{-1}. The developed biosensor exhibits attractive performance for the analysis of SirT1, with rapid response, high sensitivity, and high accuracy, and could become a promising technique for protein detection.

Human sirtuin 1 (SirT1) belongs to the mammalian SirT family and is closely related to yeast Sir2. Interest in SirT1 has grown since the initial reports that the *Saccharomyces cerevisiae* and *Caenorhabditis elegans* orthologues mediate the effects of calorie restriction (CR) to extend the lifespan of these organisms [1]. Much research has indicated that SirT1 plays a role in a wide range of cellular processes, including metabolism, cell cycle, cell growth and differentiation, apoptosis, and cellular response to stress [2], and has been shown to reduce age-associated physiological changes in mice [3,4]. Taking stock of key numbers of SirT1 in cell and molecular biology enables back-of-the-envelope calculations that test and sharpen our understanding of cellular processes [5]. Therefore, to clarify the functions of SirT1, the development of effective methods for quantitative analysis of this protein has tremendous importance in clinical diagnosis and drug screening. Up to now, instrumental methods such as Western blot [6], enzyme-linked immunosorbent assay (ELISA) [7], and reverse transcription polymerase chain reaction (RT–PCR) [8] all have been used for the study of protein evaluation. However, most methods often necessitate sophisticated instrumentation and clinically unrealistic expense and time.

Immunoassay of proteins has become an important solution for the bioanalytical problems in various fields such as disease diagnosis. The increasing demand for the screening of diseases at their early stage requires the ultrasensitive detection of biologically relevant species at an extremely low level of expression [9,10]. Thus, great efforts currently have been centered on the development of novel and effective strategies to produce and amplify signal readout. Some successful signal amplification strategies include the employment of new redox-active probes, the integration of

Abbreviations used: SirT1, sirtuin 1; PNC, polymeric nanocomposite; TiO_2, titanium dioxide; Au, gold; HAP, hyperbranched azo-polymer; $Ab_1^{\#1}$, goat polyclonal anti-SirT1; $Ab_1^{\#2}$, rabbit polyclonal anti-SirT1; Ab_2, secondary antibody; HRP, horseradish peroxidase; NHS, *N*-hydroxysuccinimide; EDC, 1-ethyl-3-3(3-dimethylaminopropyl) carbodiimide; SPDP, *N*-succinimidyl-3-(2-pyridyldithiol) propionate; PTMP, pentaerythritol tetrakis(3-mercaptopropionate); THPC, tetrakis (hydroxymethyl) phosphonium chloride; BSA, bovine serum albumin; $HAuCl_4$, chloroauric acid; PBS, phosphate buffer solution; EDX, energy dispersive X-ray; SEM, scanning electron microscopy; TEM, transmission electron microscopy; ICP–AES, inductive coupled plasma–atomic emission spectroscopy; UV, ultraviolet; SCE, saturated calomel electrode; ITO, indium tin oxide; DMSO, dimethyl sulfoxide; DTT, dithiothreitol; PDOP, polydopamine; MACA, mercaptoacetic acid; H_2O_2, hydrogen peroxide; AFM, atomic force microscopy; EIS, electrochemical impedance spectroscopy; DPV, differential pulse voltammetry.

E-mail address: anyarui@usst.edu.cn.

http://dx.doi.org/10.1016/j.ab.2016.05.020
0003-2697/

enzyme-assisted labels, and the incorporation of nanomaterials to increase the load of electrochemical tags [11,12]. In spite of many important achievements, enormous efforts on efficient signal amplification approaches are still needed to focus on improving the analytical performance and broadening the applications for immunoassay. The polymeric nanocomposites (PNCs) of polymer, nanoparticles, and more components have drawn much attention for their obvious technical and scientific interests in many fields such as biosensing. The main advantages of PNCs as biomaterials are as follows. First, the polymer matrix with high functionality and processability can efficiently entrap and adsorb the species of interest such as biomolecules [13] and nanoparticles [14]. Second, nanoparticles with significant adsorbability and biocompatibility can provide PNCs with abundant sites to bind biomolecules and retain the bioactivity [15,16]. Third, the incorporation of plenty of nanoparticles can endow PNCs with diversified functions for developing biodevices involving catalysis, electronics, optics, and magnetics. Fourth, PNCs are cost-effective, stable, and convenient to prepare [17,18].

In this article, we report an investigation of a novel immunoassay approach using hyperbranched polymer hybrids cooperating with titanium dioxide–gold (TiO_2–Au) nanocomposite as electrochemical labels to assay SirT1. Hyperbranched polymers become very intriguing with regard to design, synthesis, and functional property because of their unique and highly branched structures and a large number of terminal functional groups that show characteristics such as globular molecular shapes, high solubility, and the feasibility to be further modified through various chemical reactions of the peripheral groups [19]. The unique properties make them a prominent application for bioassay design. Here, unimolecular nanoparticles of crosslinked hyperbranched azo-polymer (HAP) decorated with Au colloids via covalent bond were used as a biosensing platform and have been demonstrated to anchor larger amounts of capture antibodies with high stability and bioactivity. The typical sandwich-type immunoassay procedure comprised the immunoreaction of capture antibody (goat polyclonal anti-SirT1, $Ab_1{}^{\#1}$) with target SirT1, followed by the attachment of detection antibody (rabbit polyclonal anti-SirT1, $Ab_1{}^{\#2}$), and {TiO_2–Au/Ab_2–HRP} labels, which featured secondary antibody horseradish peroxidase (Ab_2–HRP) linked to TiO_2–Au nanocomposites as electrochemical label. The SirT1 concentration, which was proportional to that of the Ab_2 linked to TiO_2–Au nanocomposites, could be readily examined through measurement of the electrochemical current. The proposed electrochemical measurement showed good performance in the monitoring of SirT1, which provides a promising approach to detect other significant proteins in the future.

Materials and methods

Chemicals and materials

N-Hydroxysuccinimide (NHS), 1-ethyl-3-3(3-dimethylaminopropyl) carbodiimide (EDC), dopamine, thionine, hydroxylamine hydrochloride, *N*-succinimidyl-3-(2-pyridyldithiol) propionate (SPDP), pentaerythritol tetrakis(3-mercaptopropionate) (PTMP), tetrakis (hydroxymethyl) phosphonium chloride (THPC), SirT1, goat anti-rabbit IgG-peroxidase (Ab_2–HRP), and bovine serum albumin (BSA) were all purchased from Sigma–Aldrich (St. Louis, MO, USA). Goat polyclonal anti-SirT1 ($Ab_1{}^{\#1}$) and rabbit polyclonal anti-SirT1 ($Ab_1{}^{\#2}$) were supplied by Santa Cruz Biotechnology (Santa Cruz, CA, USA). Hyperbranched polymer was a gift from Liang Ding (Department of Chemistry, East China Normal University). TiO_2 (P-25, Φ = 30 nm) was purchased from Degussa. Chloroauric acid ($HAuCl_4$), trisodium citrate, and methanol were obtained from China National Medicines (China). Disodium hydrogen phosphate, potassium dihydrogen phosphate, and hydrogen peroxide (30% [w/v] solution) were purchased from Shanghai Chemical Reagent (China). Phosphate buffer solutions (PBSs) with different pH values were prepared by using Na_2HPO_4 and KH_2PO_4. Doubly distilled water was used throughout the experiments.

Apparatus and instruments

Scanning electron microscopy (SEM) was carried out on an S-4800 (Hitachi, Tokyo, Japan) equipped with an energy dispersive X-ray (EDX) analyzer. The transmission electron microscopy (TEM) images were performed by using a transmission electron microscope (JEOL model JEM 2100, Japan). The morphologies of the polymers were studied on a BioScope atomic force microscope (NanoScope IIIa SPM System, Digital Instruments, Veeco Instruments, USA). The element compositions of the products were measured by inductive coupled plasma–atomic emission spectroscopy (ICP–AES) on an iCAP 6300 (Thermo Fisher, Waltham, MA, USA). Light absorption was measured using an ultraviolet (UV)–visible spectrophotometer (Cary 50, Varian, USA). Electrochemical experiments were achieved on a CHI 660D electrochemical system (CH Instruments, China) with a conventional three-electrode system comprising a platinum wire as auxiliary electrode, a saturated calomel electrode (SCE) as reference electrode, and a bare or modified indium tin oxide (ITO) electrode as working electrode.

Synthesis of Au–HAP hybrids

Synthesis of unimolecular nanoparticle of crosslinked HAP

HAP (200 mg) and PTMP (12.2 mg) (1:2.5 M ratio) were dissolved in 250 ml of dried tetrahydrofuran (THF) at room temperature under nitrogen atmosphere. 1-Dodecylamine (1 mg, 10 wt%) was added as a catalyst, and the mixture was stirred for 2 h. The solution was concentrated under vacuum and precipitated into an excess of ethyl acetate, and the precipitate was isolated and dried under vacuum for 24 h to give the polymer as a solid.

Conjugation of Au colloids onto the unimolecular nanoparticle of crosslinked HAP

Gold colloid solution (1–2 nm in diameter) was prepared by the reduction of chloroauric acid with THPC as described by Duff and coworkers [20]. In a typical synthesis, 1 ml of the Au solution was diluted in 15 ml of doubly distilled water. Then, 10 ml of acetone dissolved in 0.5 mg of unimolecular nanoparticles of crosslinked HAP was added dropwise into the gold colloid solution under vigorous stirring; this process was conducted under the protection of a nitrogen atmosphere to minimize the oxidation of thiol groups. After 12 h of equilibration at room temperature, the solution mixture was centrifuged at 10,000 rpm for 30 min at room temperature and the supernatant solution was discarded. The sediments were then redispersed in doubly distilled water and centrifuged again. This purification cycle was repeated three times.

Preparation of TiO_2–Au nanocomposite

TiO_2–Au nanocomposites were prepared as follows. Commercial type Degussa P-25 TiO_2 composed of 70% anatase and 30% rutile was used in the fabrication experiments. TiO_2 solution was prepared by dispersing 3 mg of TiO_2 particles (P-25) in 35 ml of doubly distilled water and sonicated for 5 min. The TiO_2 solution was stirred with 1.88 ml of sodium citrate (0.1 mol L^{-1}) for 10 min to exchange hydroxyl ion with citrate anions [21]. Then, 0.125 ml of

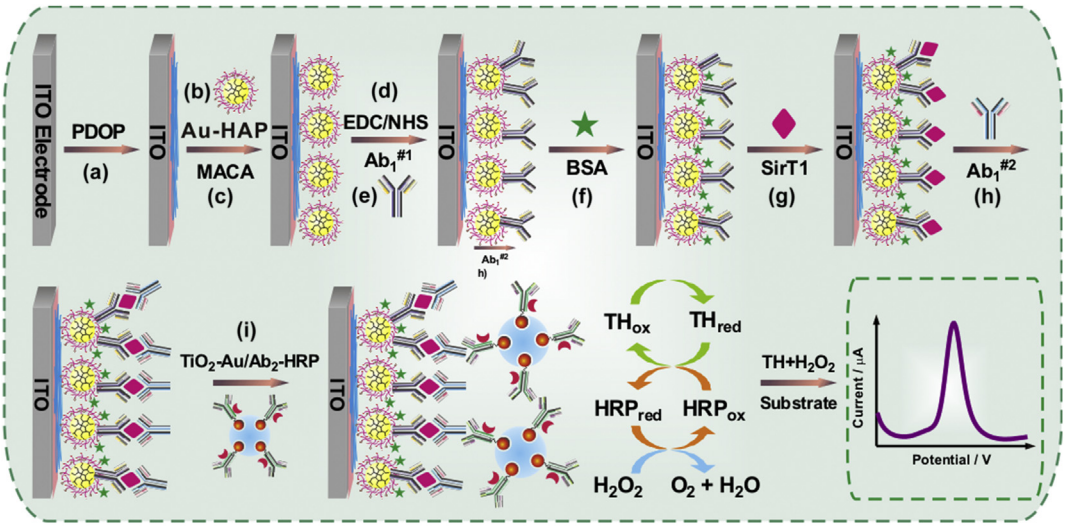

Scheme 1. Procedure for synthesis of the {TiO_2–Au/Ab_2–HRP}/$Ab_1^{\#2}$/SirT1/$Ab_1^{\#1}$/Au–HAP/PDOP/ITO immunosensor. TH, thionine.

$HAuCl_4$ (1%) was incrementally added (with at least 10 min between additions) along with an excess of 0.07 ml $NH_2OH \cdot HCl$ (0.1 mol L^{-1}). After stirring for approximately 12 h, the clear solution became purple and TiO_2–Au nanocomposites were synthesized. Subsequently, the TiO_2–Au nanocomposites were purified by centrifuging and redispersing in 10 ml of doubly distilled water.

Preparation of {TiO_2–Au/Ab_2–HRP} labels

Thiolated Ab_2–HRP was prepared according to the previous protocol [22], where 2.0 mg of Ab_2–HRP was dissolved in 100 μl of pH 7.4 PBS, followed by the addition of 2.0 mg of SPDP dissolved in 10 μl of dimethyl sulfoxide (DMSO). After stirring for 1.5 h at room temperature, 10 μl of dithiothreitol (DTT, 1 mol L^{-1}) was added to the mixture. The reduction was performed under nitrogen with stirring at room temperature for 30 min. The reduced SPDP–Ab_2–HRP was filtered through a Microseppall and then dispersed in 100 μl of pH 7.4 PBS. Thereafter, the reduced SPDP–Ab_2–HRP was added to 1.0 ml of TiO_2–Au nanocomposite solution. The mixture was incubated at room temperature with gentle mixing for 12 h and then blocked by BSA solution (100 μl, 1%) for 30 min. The solution was centrifuged at 10,000 rpm for 20 min at 4 °C. After centrifugation, the supernatant was removed and the soft sediment was washed with PBS (0.01 M, pH 7.4) and then resuspended in 500 μl of pH 7.4 PBS. The resulting {TiO_2–Au/Ab_2–HRP} labels were stored at 4 °C when not in use.

Preparation of electrochemical immunosensor

The electrochemical immunosensors were fabricated on diced ITO electrodes (1.5 × 0.5 cm each). Briefly, the ITO electrodes were sonicated in acetone, NaOH (1 M) of ethanol/water mixture (1:1, v/v), and water, respectively, for 15 min each. The fabrication procedure of the immunosensor is shown in Scheme 1. First, polydopamine (PDOP) was coated on ITO glass according to the literature [23]. Next, 0.50 mg ml^{-1} dopamine was dissolved in 10 mmol L^{-1} pH 8.5 Tris–HCl, and ITO slices were dipped into the solution for 12 h (Scheme 1a). The coated surfaces were rinsed with water and dried by nitrogen to get PDOP/ITO [24]. Afterward, the PDOP/ITO was immersed into the Au–HAP hybrid solution for 12 h to obtain Au–HAP/PDOP/ITO (Scheme 1b). The electrode was then immersed into mercaptoacetic acid (MACA) aqueous solution (2 mM) for 12 h at 4 °C (Scheme 1c). The carboxyl groups of MACA were activated by 10 μl of aqueous solution containing EDC (2 mM) and NHS (5 mM), followed by rinsing with deionized water (Scheme 1d). Thereafter, the activated electrode was immersed into 5 μl of $Ab_1^{\#1}$ solution for 1 h to yield the $Ab_1^{\#1}$/Au–HAP/PDOP/ITO (Scheme 1e). The resulting electrode was washed with PBS (0.01 M, pH 7.4) and then blocked with BSA (10 μl, 1.5%) for 30 min at room temperature (Scheme 1f). Then, 5 μl of various concentrations of target SirT1 samples was dropped onto the $Ab_1^{\#1}$/Au–HAP/PDOP/ITO electrodes for 1 h at 37 °C (Scheme 1g). After that, the electrodes were incubated in 5 μl of $Ab_1^{\#2}$ solution for 1 h at 37 °C to form $Ab_1^{\#2}$/SirT1/$Ab_1^{\#1}$/Au–HAP/PDOP/ITO (Scheme 1g). The obtained electrodes were dipped into 5 μl of {TiO_2–Au/Ab_2–HRP} label suspension for 1 h (Scheme 1i). Finally, the electrodes were washed thoroughly with PBS to remove nonspecifically bound labels and then stored at 4 °C prior to use.

Electrochemical measurements

The electrochemical measurements were carried out in a standard three-electrode system using a CHI 660D electrochemical system. The modified ITO electrode acted as a working electrode, an SCE as a reference electrode, and a Pt wire as a counter electrode. All electrochemical responses of the immunosensor were performed in degassed pH 6.5 PBS containing thionine (1.0 mM) and hydrogen peroxide (H_2O_2, 2.0 mM) by applying a potential of −0.2 V on the immunosensor at room temperature.

Results and discussion

Characterization of Au–HAP hybrids

The interaction between gold colloids and unimolecular nanoparticle of crosslinked HAP was demonstrated with UV–visible absorption spectroscopy. Curves a and b in Fig. 1 show the absorption spectra of the dispersed gold colloids and the unimolecular nanoparticle of crosslinked HAP, respectively. Apparently, gold colloids displayed a typical characteristic of the surface

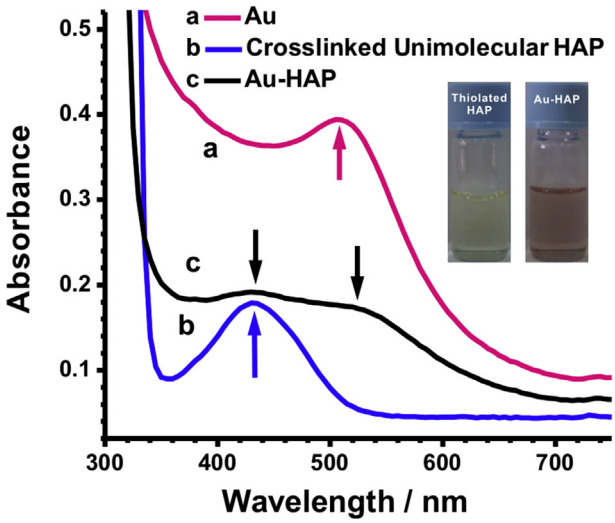

Fig.1. UV–visible absorption spectra of gold colloids (a), unimolecular nanoparticle of crosslinked HAP (b), and Au–HAP hybrids (c). Inset: photographs of unimolecular nanoparticle of crosslinked HAP (left) and Au–HAP nanocomposites (right).

plasmon band at approximately 505 nm. The characteristic peak of unimolecular nanoparticle of crosslinked HAP appeared at 432 nm, which corresponds to the $n \rightarrow \pi^*$ transition in the polymer. After the unimolecular nanoparticle of crosslinked HAP had been decorated with gold colloids, several absorption peaks along with further broadening of the absorption band and an increase in the baseline because of scattering effects were simultaneously observed (Fig. 1C). The peak at 432 nm was mainly ascribed to the unimolecular nanoparticle of crosslinked HAP, in contrast with that of pure unimolecular nanoparticle of crosslinked HAP. In addition, a remarkable shift of the gold absorption band at 505 nm toward a higher wavelength (520 nm) was observed, which was assigned to an aggregation of the decorated gold colloids. The results suggested that gold colloids could be covalently conjugated onto the surface of unimolecular nanoparticle of crosslinked HAP through thiol group interactions.

The diameter of the polymer nanoparticles was investigated by atomic force microscopy (AFM) images. As shown in Fig. 2A, the unimolecular nanoparticles of crosslinked HAP are uniform and well dispersed, exhibiting an average diameter of approximately 32.9 nm. After the unimolecular nanoparticle of crosslinked HAP was decorated with gold colloids to form Au–HAP hybrids, the average diameter increased to 42.8 nm (Fig. 2B). The morphologies and microstructures of the Au–HAP hybrids were further confirmed by TEM images (Fig. 2C); the presence of robust gold colloid clusters can be observed. Only gold colloid clusters can be seen because the unimolecular nanoparticle of crosslinked HAP exhibits considerably lower attenuation effect to electron beams compared with that exhibited by gold colloids. The morphology of gold colloid clusters is almost circular, and the size is generally comparable to the size of the Au–HAP hybrids as determined by AFM. The result clearly confirmed that the covalently conjugated gold colloids served as a good indicator for directly visualizing the dimensions of hyperbranched polymer nanoparticles.

Characterization of TiO_2–Au nanocomposites

The samples of the original TiO_2 (P-25) and TiO_2–Au nanocomposites were characterized by SEM and TEM to obtain information about morphologies and microstructures. In Fig. 3B, it can be clearly observed that the Au nanopaticles were loaded on the surface of TiO_2 particles (arrows), and they were dispersed evenly throughout the TiO_2 particles compared with the original TiO_2 (Fig. 3A). The result confirms the successful deposition of Au nanoparticles on TiO_2 particles. Fig. 3C shows the TEM images of the P-25 TiO_2 particles, which are uniform with a mean diameter of 30 nm. The Au nanoparticles can be more easily found in bright-field TEM images (Fig. 3D), showing that Au nanoparticle were deposited on TiO_2. It can also be observed that the nanometer-sized Au nanoparticle in the range of 5–8 nm were highly dispersed with mostly narrow size distributions. EDX analysis further confirmed the presence of Au along with Ti and O (see Fig. 3E below). The nanoparticle sample prepared can reach an Au loading of 2 wt% as analyzed by ICP–AES.

Electrochemical behavior of immunosensor

Electrochemical impedance spectroscopy (EIS) is an effective technique for probing the surface features of modified electrodes to understand the chemical transformations and processes associated with the conductive electrode surface. The stepwise construction process of the immunosensor was characterized by EIS as shown in Fig. 4A. The bare ITO displayed a very small semicircle (curve a), whereas the electron transfer resistance (R_{et}) remarkably increased after PDOP formed on the ITO surface (curve b). After PDOP/ITO electrode was modified with Au–HAP, the electrode showed a higher resistance for the redox probe (curve c), implying that Au–HAP blocked the electron exchange between the redox probe and the electrode. Subsequently, the capture antibody ($Ab_1{}^{\#1}$), SirT1, and the detection antibodies ($Ab_1{}^{\#2}$) were constructed on the surface of Au–HAP/PDOP/ITO step by step, and the R_{et} of each related electrode increased correspondingly (curves d–f). In addition, the access of the redox probe to the electrode surface was hindered after incubation with {TiO_2–Au/Ab_2–HRP} labels, causing an obvious increase of EIS owing to the semiconductor nature of TiO_2 and the insulating property of protein (curve g). The cyclic

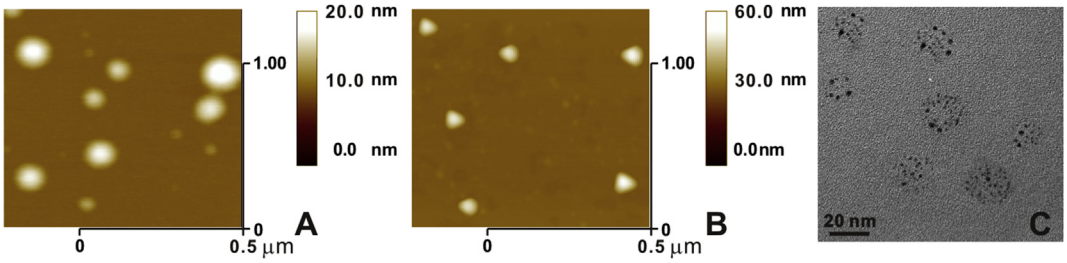

Fig.2. (A,B) AFM images of unimolecular nanoparticle of crosslinked HAP (A) and Au–HAP hybrids (B) on mica plates. (C) TEM images of Au–HAP hybrids.

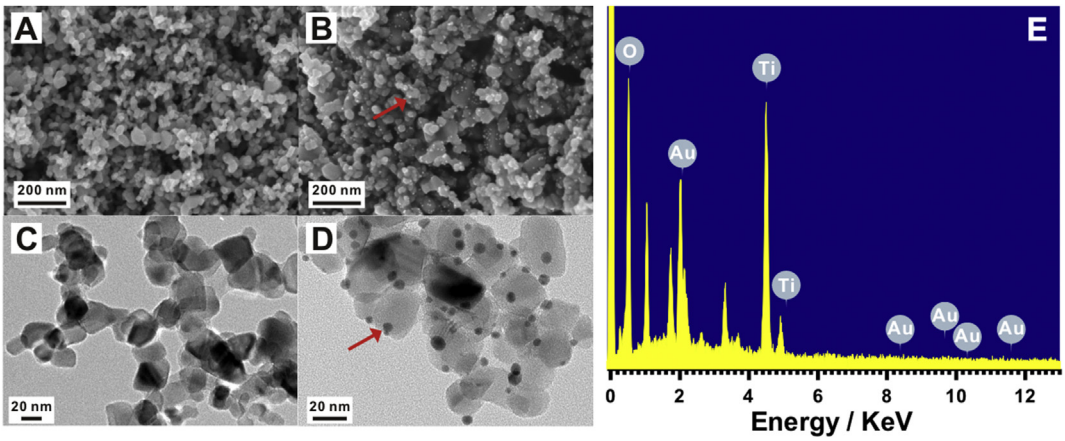

Fig.3. (A,B) Typical SEM images of samples: (A) original TiO_2 (P-25); (B) TiO_2–Au nanocomposites. (C,D) Typical TEM images of samples: (C) original TiO_2 (P-25); (D) TiO_2–Au nanocomposites. (E) EDX spectra of TiO_2–Au nanocomposites.

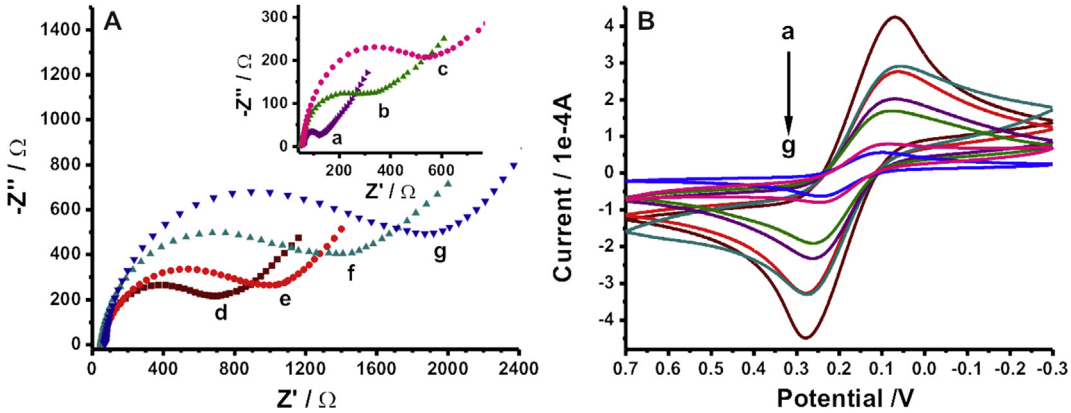

Fig.4. Nyquist plots of EIS with amplitude of 5 mV and frequency range of 0.1 Hz–100 kHz (A) and cyclic voltammograms for fabrication steps (B): (a) bare ITO, (b) PDOP/ITO, (c) Au–HAP/PDOP/ITO, (d) $Ab_1^{\#1}$/Au – HAP/PDOP/ITO, (e) SirT1/$Ab_1^{\#1}$/Au–HAP/PDOP/ITO, (f) $Ab_1^{\#2}$/SirT1/$Ab_1^{\#1}$/Au–HAP/PDOP/ITO, and (g) {TiO_2–Au/Ab_2–HRP}/$Ab_1^{\#2}$/SirT1/$Ab_1^{\#1}$/Au–HAP/PDOP/ITO, which were measured in pH 7.4 PBS containing 5.0 mM $FeCN_6^{3-/4-}$.

voltammetry in Fig. 4B also illustrates the changes accompanying the stepwise electrode modification process. The results obtained completely coincided with those from EIS, which further confirmed the success in design of the proposed immunosensor.

Optimal conditions for electrochemical detection

The parameters of the concentrations of thionine and H_2O_2 played an important role in the enzymatic catalytic reaction. Fig. 5A

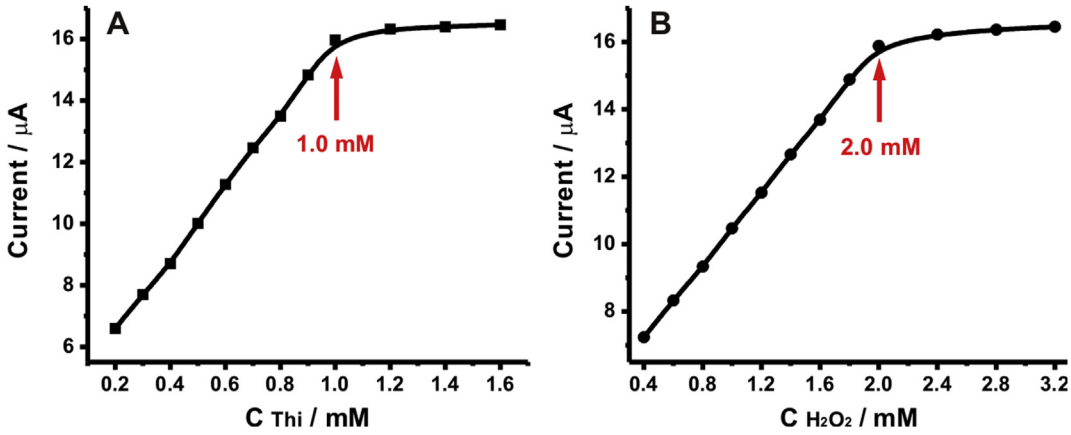

Fig.5. Effects of concentrations of thionine (Thi) (A) and H_2O_2 (B) on the electrochemical responses of the immunosensor toward 100 ng ml^{-1} SirT1 in pH 6.5 PBS.

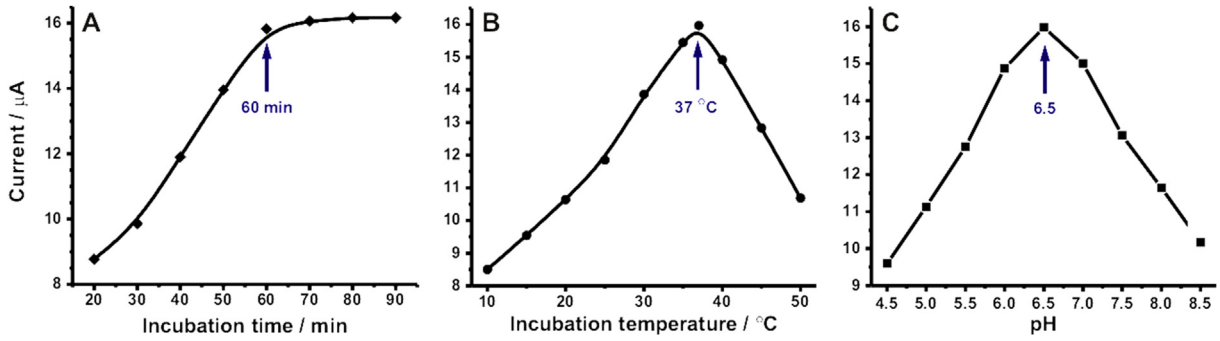

Fig.6. Effects of incubation time (A), incubation temperature (B), and pH of detection solution (C) on the electrochemical responses of the immunosensor toward 100 ng ml^{-1} SirT1 in pH 6.5 PBS.

shows the dependence of thionine concentration on the current in pH 6.5 PBS. With the increasing concentration of thionine, the current increased and reached a maximum response at the thionine concentration of 1.0 mM. Thus, the concentration of 1.0 mM was chosen for use in the following assay. The effect of the H_2O_2 concentration on the electrochemical enzyme-catalyzed reaction was also examined, as shown in Fig. 5B. It can be seen that the current value increased when the H_2O_2 concentration was in the range from 0.4 to 3.2 mM and then started to level off, which corresponded to the saturated station. Therefore, the optimal concentration of H_2O_2 was chosen at 2.0 mM.

Optimization of conditions for immunoreaction

In the immunoassays, time and temperature for the antigen–antibody interaction greatly influence the sensitivity of the developed immunosensor. In Fig. 6A, the amperometric responses increased with the incubation time and then tended to constant values after 60 min, which showed a saturated binding between the antigen and the primary antibody on electrode surface. Therefore, subsequent experiments employed 60 min as the optimal time for all of the incubation steps of the assay. At the optimized time, with an increasing incubation temperature from 10 to 50 °C, the immunosensor showed a maximum current response at 37 °C in pH 6.5 containing 1.0 mM H_2O_2 after incubation with 100 ng ml^{-1} of SirT1 (Fig. 6B). The temperatures over 37 °C resulted in a deterioration of amperometric response. The reason may be that the high temperature caused an irreversible behavior (denaturation of HRP) involved in the process. Furthermore, the temperatures lower than 37 °C could reduce the immunoreaction rate, thereby lengthening the incubation time. Consequently, the temperature of 37 °C was selected for further studies. The pH value of the detection solution was also investigated in the enzymatic response (Fig. 6C). The amperometric response increased steeply with the increasing pH value from 5.0 to 6.5 and then decreased when the pH was over 6.5. Thus, pH 6.5 PBS was selected as the detection solution for SirT1 immunoassay.

Analytical performance for determination of SirT1

Fig. 7 depicts the calibration curve for SirT1 assay using Au–HAP as biosensor platform and {TiO_2–Au/Ab_2–HRP} as electrochemical labels under optimal conditions. Measurements were performed in triplicate using three different immunosensors at each concentration. As the concentration of SirT1 increased, the amperometric response was enhanced accordingly (Fig. 7A). The calibration plot shows a good linear relationship between the amperometric response and the SirT1 concentration in the range from 1.0 to 500 ng ml^{-1} with a correlation coefficient of 0.9968. The linear curve fits a regression equation of $y = 0.1426x + 1.5021$. The detection limit of this method was estimated to be 0.28 ng ml^{-1} based on 3 SD/m, where SD is the standard deviation of the

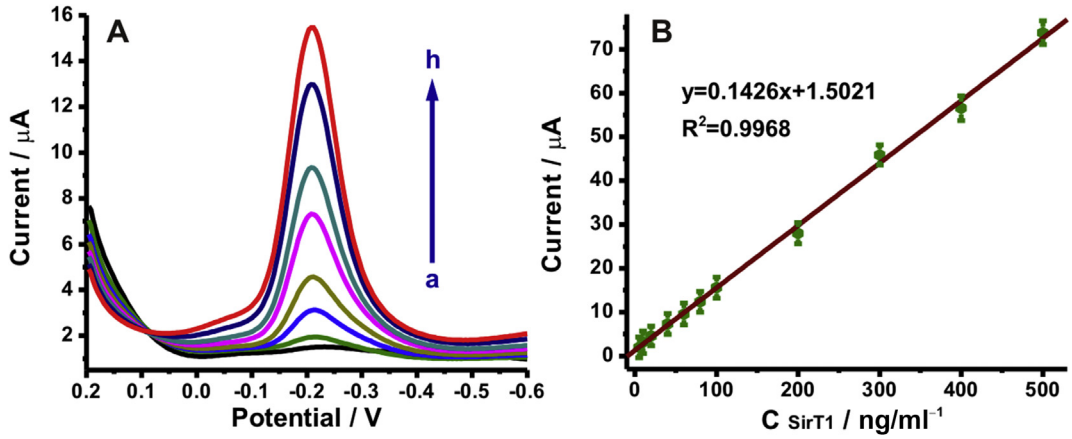

Fig.7. (A) DPV responses of {TiO_2–Au/Ab_2–HRP}/$Ab_1{}^{\#2}$/SirT1/$Ab_1{}^{\#1}$/Au–HAP/PDOP/ITO immunosensor analyzing with different concentrations of SirT1 under optimized conditions: (a) 0 ng ml^{-1}; (b) 5 ng ml^{-1}; (c) 10 ng ml^{-1}; (d) 20 ng ml^{-1}; (e) 40 ng ml^{-1}; (f) 60 ng ml^{-1}; (g) 80 ng ml^{-1}; (h) 100 ng ml^{-1}. (B) Calibration curve obtained with {TiO_2–Au/Ab_2–HRP}/$Ab_1^{\#2}$/SirT1/$Ab_1^{\#1}$/Au–HAP/PDOP/ITO immunosensor analyzing with different concentrations of SirT1.

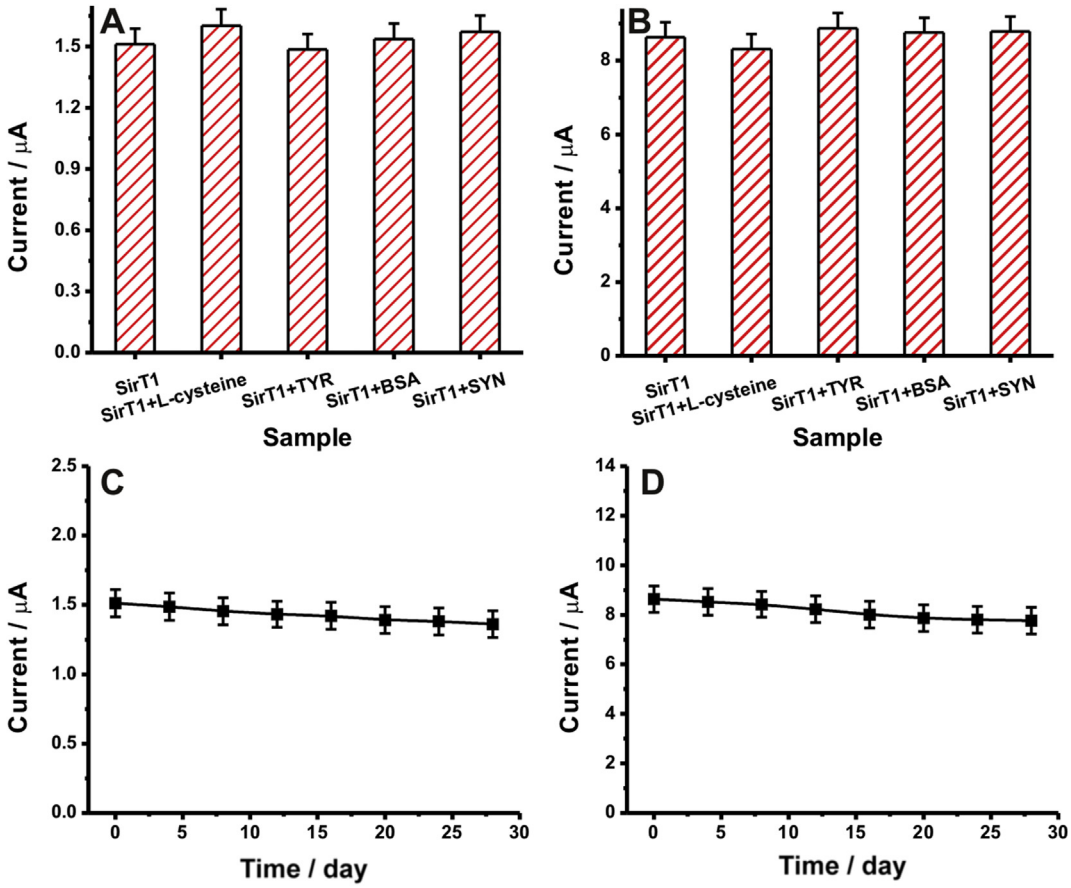

Fig.8. (A,B) Current response of immunosensor to 50 ng ml^{-1} SirT1 + 500 ng ml^{-1} interferences in pH 7.4 PBS in the absence (A) and presence (B) of thionine and H_2O_2 ($n = 3$). TYR, tyrosinase; SYN, α-synuclein. (C,D) Variation of the response current versus storage time at 4 °C in the absence (C) and presence (D) of thionine and H_2O_2.

measurements of noncomplementary target solutions and *m* is the slope of the plot in Fig. 7B. The results illustrate that the greatly increased sensitivity relies on the dual signal amplification strategy.

Selectivity, stability, and reproducibility of immunosensor

Possible interfering substances were used to evaluate the selectivity of the proposed immunosensor. As shown in Fig. 8A and B, the immunosensors were incubated with 50.0 ng ml^{-1} SirT1 solution containing 500 ng ml^{-1} of the interference of L-cysteine, tyrosinase (TYR), BSA, and α-synuclein (SYN). There is no remarkable change in differential pulse voltammetry peak current based on the fabricated method for the mixture in comparison with individual SirT1 solution. Therefore, it can be concluded that the selectivity of the proposed immunosensor was acceptable.

The stability of the immunosensor is a key factor in developing a good immunosensor. As shown in Fig. 8C and D, the stability of the {TiO_2–Au/Ab_2–HRP}/$Ab_1{}^{\#2}$/SirT1/$Ab_1{}^{\#1}$/Au–HAP/PDOP/ITO immunosensor was tested by recording the DPV responses every 4 days for 1 month for electrodes stored in PBS at 4 °C. After 1 month of storage, the amperometric responses still retained 90.9% value of the initial response, indicative of a quite satisfying stability.

The reproducibility of the proposed immunosensor was evaluated through analysis of five independently made immunosensors. The current response gave a relative standard deviation (RSD) of 3.3% toward 100 ng ml^{-1} SirT1, which indicated an acceptable reproducibility and precision of the fabrication protocol described above.

Table 1
The recovery experiment in cell samples.

Cell sample	Added value (ng ml^{-1})	Found value (ng ml^{-1})	Recovery (%)
1	5.00	5.22	104.4
2	10.0	10.78	107.8
3	20.0	19.37	96.85
4	40.0	39.10	97.75
5	60.0	62.16	103.6

Recovery and application of proposed immunosensor

To investigate the possibility of the novel developed method being applied to real samples, the recovery experiments were performed by standard addition methods. The standard samples of SirT1 were dissolved in the H1299-E2F1-ER cell samples (the concentration range of SirT1 was 5.00–60.0 ng ml^{-1}) and detected the SirT1 in cell samples. The experimental results are shown in Table 1, and the recoveries obtained are in the range from 94.45 to 107.8%, indicating that the immunosensor could be effectively applied to the determination of SirT1 in real samples.

Conclusion

We have demonstrated that highly sensitive electrochemical detection of SirT1 with {TiO_2–Au/Ab_2–HRP} labels cooperated with Au–HAP polymer. The novelty consists in the immobilization of Au–HAP polymer film as an anchoring layer as well as TiO_2–Au

nanocomposites as “electrochemical labels.” The proposed electrochemical measurement showed good performance in the monitoring of SirT1 with a rapid response, wide concentration range, and high sensitivity. It is expected that the designed strategy will evolve toward a very promising future for reliable diagnostics of cancer and other diseases and as tools for intra-operation pathological testing, proteomics, and systems biology.

Acknowledgments

We gratefully acknowledge the National Natural Science Foundation of China (21505092). We also thank University of Shanghai for Science and Technology for financial support: Foundation of China (D15011) and 1P16341010.

References

[1] H.A. Tissenbaum, L. Guarente, Increased dosage of a sir-2 gene extends lifespan in *Caenorhabditis elegans*, Nature 410 (2001) 227–230.
[2] S. Michan, D. Sinclair, Sirtuins in mammals: insights into their biological function, Biochem. J. 404 (2007) 1–13.
[3] C.A. Blum, J.L. Ellis, C. Loh, P.Y. Ng, R.B. Perni, R.L. Stein, SERT1 modulation as a novel approach to the treatment of diseases of aging, J. Med. Chem. 54 (2011) 417–432.
[4] (a) D. Anastasiou, W. Krek, SIRT1: linking adaptive cellular responses to aging-associated changes in organismal physiology, Physiology 21 (2006) 404–410; (b) L. Guarente, Sirtuins in aging and disease, Biology 72 (2007) 483–488.
[5] Q.J. Zhang, Z. Wang, H.Z. Chen, S. Zhou, W. Zheng, G. Liu, Y.S. Wei, H. Cai, D.P. Liu, C.C. Liang, Endothelium-specific overexpression of class III deacetylase SIRT1 decreases atherosclerosis in apolipoprotein E-deficient mice, Cardiovasc. Res. 80 (2008) 191–199.
[6] U. Moran, R. Phillips, R. Milo, SnapShot: key numbers in biology, Cell 141 (2010) 1262.
[7] F. Chu, P.M. Chou, X. Zheng, B.L. Mirkin, A. Rebbaa, Control of multidrug resistance gene *mdr1* and cancer resistance to chemotherapy by the longevity gene *sirt1*, Cancer Res. 65 (2005) 10183–10187.
[8] C. Gey, S. Kyrylenko, L. Hennig, L.H.D. Nguyen, A. Büttner, H.D. Pham, A. Giannis, Phloroglucinol derivatives guttiferone G, aristoforin, and hyperforin: Inhibitors of human sirtuins SIRT1 and SIRT2, Angew. Chem. Int. Ed. 46 (2007) 5219–5222.
[9] Y. Fu, K. Liu, Q. Sun, B. Lin, D. Lu, Z. Xu, C. Hu, G. Fan, S. Zhang, C. Wang, W. Zhang, A highly sensitive immunosensor for calmodulin assay based on enhanced biocatalyzed precipitation adopting a dual-layered enzyme strategy, Biosens. Bioelectron. 56 (2014) 258–263.
[10] G. Lai, H. Zhang, T. Tamanna, A. Yu, Ultrasensitive immunoassay based on electrochemical measurement of enzymatically produced polyaniline, Anal. Chem. 86 (2014) 1789–1793.
[11] Y. Zhao, L. Liu, D. Kong, H. Kuang, L. Wang, C. Xu, Dual amplified electrochemical immunosensor for highly sensitive detection of *Pantoea stewartii* subsp. *stewartii*, ACS Appl. Mater. Interf. 6 (2014) 21178–21183.
[12] Y. Lin, Q. Zhou, Y. Lin, D. Tang, R. Niessner, D. Knopp, Enzymatic hydrolysate-induced displacement reaction with multifunctional silica beads doped with horseradish peroxidase–thionine conjugate for ultrasensitive electrochemical immunoassay, Anal. Chem. 87 (2015) 8531–8540.
[13] H. Wang, G. Li, Y. Zhang, M. Zhu, H. Ma, B. Du, Q. Wei, Y. Wan, Nanobody-based electrochemical immunoassay for ultrasensitive determination of apolipoprotein-A1 using silver nanoparticles loaded nanohydroxyapatite as label, Anal. Chem. 87 (2015) 11209–11214.
[14] S. Weng, Q. Liu, C. Zhao, G. Hong, Z. Jiang, L. Lin, Y. Chen, X. Lin, Sensitive electrochemical immunoassay based on polythionine–Au nanocomposites as enhanced sensing signal for selective detection of biomarker with high isoelectric point, Sens. Actuators. B Chem. 216 (2015) 307–315.
[15] X. Zhang, W. Lu, J. Shen, Y. Jiang, E. Han, X. Dong, J. Huang, Carbohydrate derivative-functionalized biosensing toward highly sensitive electrochemical detection of cell surface glycan expression as cancer biomarker, J. Biosens. Bioelectron. 74 (2015) 291–298.
[16] Y. Lin, Q. Zhou, Y. Lin, M. Lu, D. Tang, Mesoporous carbon-enriched palladium nanostructures with redox activity for enzyme-free electrochemical immunoassay of brevetoxin B, Anal. Chim. Acta 887 (2015) 67–74.
[17] C.K. Tang, A. Vaze, J.F. Rusling, Paper-based electrochemical immunoassay for rapid, inexpensive cancer biomarker protein detection, Anal. Methods 6 (2014) 8878–8881.
[18] (a) B. Zhang, D. Tang, I.Y. Goryacheva, R. Niessner, D. Knopp, Anodic-stripping voltammetric immunoassay for ultrasensitive detection of low-abundance proteins using quantum dot aggregated hollow microspheres, Chem. Eur. J. 19 (2013) 2496–2503;
(b) Y. Zhao, Y. Zheng, R. Kong, L. Xia, F. Qu, Ultrasensitive electrochemical immunosensor based on horseradish peroxidase (HRP)-loaded silica-poly(acrylic acid) brushes for protein biomarker detection, Biosens. Bioelectron. 75 (2016) 383–388.
[19] L. Ding, L. Zhang, H. Han, W. Huang, C. Song, M. Xie, Y. Zhang, Hyperbranched azo-polymers synthesized by acyclic diene metathesis polymerization of an AB_2 monomer, Macromolecules 42 (2009) 5036–5042.
[20] D.G. Duff, A. Baiker, P.P. Edwards, A new hydrosol of gold clusters: 1. Formation and particle size variation, Langmuir 9 (1993) 2301–2309.
[21] Y. Qu, H. Min, Y. Wei, F. Xiao, G. Shi, X. Li, L. Jin, Au–TiO_2/Chit modified sensor for electrochemical detection of trace organophosphates insecticides, Talanta 76 (2008) 758–762.
[22] J. Zheng, B.D. Hammock, Development of polyclonal antibodies for detection of protein modification by 1,2-naphthoquinone, Chem. Res. Toxicol. 9 (1996) 904–909.
[23] H. Lee, S.M. Dellatore, W.M. Miller, P.B. Messersmith, Mussel-inspired surface chemistry for multifunctional coatings, Science 318 (2007) 426–430.
[24] G. Wang, H. Huang, G. Zhang, X. Zhang, B. Fang, L. Wang, Dual amplification strategy for the fabrication of highly sensitive interleukin-6 amperometric immunosensor based on poly-dopamine, Langmuir 27 (2011) 1224–1231.